HYGRO-MECHANICAL MODEL FOR CONCRETE PAVEMENT WITH LONG-TERM DRYING ANALYSIS

JAKUB VESELÝ*, VÍT ŠMILAUER

Czech Technical University in Prague, Faculty of Civil Engineering, Department of Mechanics, Thákurova 7, 166 29 Prague 6, Czech Republic

* corresponding author: `jakub.vesely.2@fsv.cvut.cz`

ABSTRACT. Concrete pavements are subjected to the combination of moisture transport, heat transport and traffic loading. A hygro-mechanical 3D finite element model was created in OOFEM software in order to analyse the stress field and deformed shape from a long-term non-uniform drying. The model uses a staggered approach, solving moisture transfer weakly coupled with MPS viscoelastic model for ageing concrete creep and shrinkage. Moisture transport and mechanical sub-models are calibrated with lab experiments, long-term monitoring on D1 highway and data from 40 year old highway pavement. The slab geometry is $3.5 \times 5.0 \times 0.29$ m, resting on elastic Winkler-Pasternak foundation. The validation covers autogenous and drying strain on the slab. The models predict drying-induced tensile stress up to 3.3 MPa, inducing additional loading on the slab, uncaptured by current design methods.

KEYWORDS: Concrete pavement, hygro-mechanical analysis, creep, shrinkage.

1. INTRODUCTION

Concrete pavements present a proven solution for highways and airports due to its ability to withstand high mechanical loads with long service life compared to bituminous alternatives [1]. Effects of wheel load, temperature and moisture generally need to be considered, as they influence stress, strain, deformations and service life [2]. For a detailed pavement analysis, finite element simulations with various factors have been carried out [3–7].

Hydration and moisture transport generally induces autogeneous shrinkage strain, drying shrinkage strain with an impact on creep. Early microcracks may occur due to internal or external restraints [8]. In addition, moisture gradients generate differential shrinkage between the top and the bottom, leading to warping [9, 10]. Stress relaxation plays a role on the warping effect [11].

There are several approaches for creating a thermo-hygro-mechanical model for concrete. The most simple one uses a superposition principle, solving moisture, thermal, traffic load and ASR effects separately [12]. Due to a coupled nature of the problem, a staggered solution strategy offers more accurate analysis [13], solving moisture and heat transport and passing the obtained fields to a mechanical model. Fully coupled problems with chemical submodels were proposed as well [14–16].

This paper presents a new hygro-mechanical 3D model, implemented in an open-source software OOFEM [17]. A staggered solution strategy uses solving of the weakly-coupled sub-models in the discretized time steps. The geometry uses 3D representation of a single rectangular concrete slab resting on Winkler-Pasternak foundation without dowel bars. The aim is to inspect overall performance of the concrete pavement under long-term drying loading scenario. A similar model has been published with limited calibration and interpretation [18].

2. FORMULATION OF A HYGRO-MECHANICAL MODEL

Hygro-mechanical model solves transport of moisture and mechanical behavior of the slab. Staggered solution strategy is adopted in the multiphysical model, partially separating transport transient problem from the mechanical one and passing transient moisture field to the mechanical problem. Such an approach allows to define equivalent time in creep models or to calibrate constitutive laws independently. The models were implemented in OOFEM, an open-source and object-oriented software for finite element method [17].

2.1. MOISTURE TRANSPORT

A nonlinear moisture transport model describes concrete as a single-fluid medium with the governing equation:

$$k(h)\frac{\partial h}{\partial t} = \nabla \cdot [c(h)\nabla h], \qquad (1)$$

where h is the dimensionless pore relative humidity, $k(h)$ [kg/m^3] is the humidity-dependent moisture capacity ($k(h) = \frac{\partial w}{\partial h}$) which is derivative of the moisture content $w(h)$ [kg/m^3] with respect to the relative humidity), $c(h)$ [kg/m/s] is the moisture permeability in the Bažant-Najjar's form:

$$c(h) = c_1 \left(\alpha_0 + \frac{1 - \alpha_0}{1 + \left(\frac{1-h}{1-h_c}\right)^n} \right). \qquad (2)$$

Newton (convection) boundary condition is used in the form $q_n = \beta(h - h_\infty)$ with the moisture transfer coefficient β.
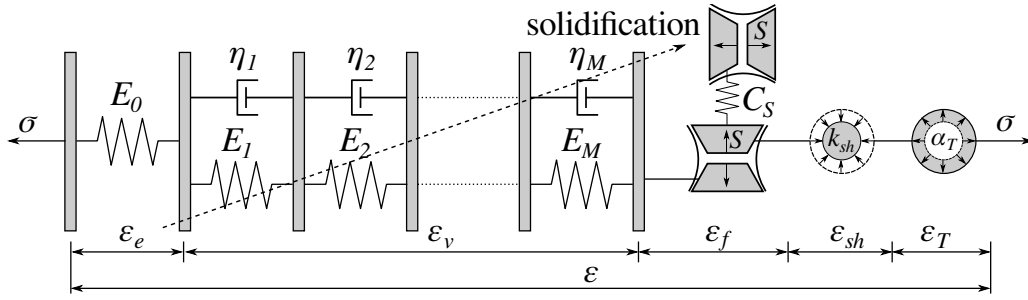
FIGURE 1. Rheological scheme of MPS model.

2.2. MECHANICAL MODEL

The mechanical model consists of three different components. The first one takes a concrete slab with a viscoelastic model for concrete with ageing based on microprestress solidification theory (MPS) [19]. The slab is placed on elastic, 2D subsoil, Winkler-Pasternak model. The interaction between the slab and the subsoil is controlled by interface elements.

2.2.1. LINEAR VISCOELASTIC MATERIAL MODEL FOR CREEP AND SHRINKAGE

A constitutive model for creep and shrinkage originate from B3 model [20] extended with MPS formulation [19]. The rheological model in Figure 1 shows non-aging asymptotic elastic spring, solidifying Kelvin chain, aging dashpot, shrinkage strain, and thermal strain. The viscosity η_f in the flow strain ε_f depends on the evolution of the microprestress. All these units are connected in series, manifesting total strain decomposition into individual contributions. The governing equation for MPS theory reads [21]:

$$\dot{\eta}_f + \frac{1}{\mu_S T_0} \left| \dot{T} \ln h + \frac{\dot{h}}{h} \right| (\mu_S \eta_f)^{\frac{p}{p-1}} = \frac{\psi_S}{q_4}, \quad (3)$$

where μ_S is a parameter with the dimension of fluidity, p is a dimensionless material parameter influencing the size effect (for $p = \infty$, the size effect disappears), ψ_S is a temperature and humidity dependent factor, q_4 is a material parameter, T is the current temperature, and T_0 is the reference temperature. Equation (3) can be simplified into Equation (4) under the assumption of constant temperature $T = T_0$ as:

$$\dot{\eta}_f + k_3 \left| \frac{\dot{h}}{h} \right| \eta_f^{\tilde{p}} = \frac{\psi_S}{q_4}, \quad (4)$$

with parameters:

$$\tilde{p} = \frac{p}{p-1}, \quad (5)$$

$$k_3 = \mu_S^{\frac{1}{p-1}}. \quad (6)$$

The drying shrinkage is computed as:

$$\dot{\varepsilon_{sh,d}} = k_{sh} \dot{h}, \quad (7)$$

with shrinkage ratio k_{sh}. The autogenous shrinkage $\varepsilon_{sh,au}$ is approximated as:

$$\varepsilon_{sh,au} = \varepsilon_{sh,au}^{\infty} \left[1 + (\tau_{au}/t_e)^{\frac{w/c}{0.38}} \right]^{R_{t,au}}, \quad (8)$$

where $\varepsilon_{sh,au}^{\infty}$ is the ultimate value of autogenous shrinkage strain, w/c is water/cement ratio and parameters $\tau_{au}, R_{t,au}$ control strain evolution in time t_e.

2.2.2. WINKLER-PASTERNAK SUBSOIL MODEL

Elastic subsoil is treated as a 2D Winkler-Pasternak model, capturing normal and shear stiffness with c_1 and c_2 parameters [22–24]. The governing equation reads:

$$f(z) = c_1 w(z) - c_2 \frac{\partial^2 w(z)}{\partial z^2}, \quad (9)$$

where $f(z)$ is surface load and $w(z)$ is displacement.

2.2.3. INTERFACE ELEMENTS

The interface elements allow separation between the slab and subsoil, eliminating tension stress. Both meshes of slab and subsoil share coinciding nodes at the interface. The traction-separation law takes the form:

$$\begin{aligned} t_n &= k_n \delta, \\ k_n &= k \quad \text{for compression}, \\ k_n &= 0.01k \quad \text{for tension}, \end{aligned} \quad (10)$$

where δ is displacement between two nodes, positive in separation. Shear stiffness is assumed zero. Interface elements lead generally to slower converge or even convergence loss hence it is important to use reasonable time step to induce gradual slab deformations.

3. RESULTS AND DISCUSSION

The presented numerical model stems from a monitored highway slab. The pilot project started in 2017 as a joint activity among the Road and Motorway Directorate (ŘSD ČR), a contractor Skanska, a.s. and the Czech Technical University in Prague [25]. The project involved 8 978 m of concrete pavement built on D1 highway Přerov-Lipník nad Bečvou, the Czech Republic. The pavement was cast between 07/2018 and 09/2019 with the opening to traffic Dec 12, 2019. The binder used a slag-blended, slow hardening binder composed of 75 % CEM I 42.5 R(sc) + 25 % GGBFS SMŠ 400, corresponding to CEM II/B-S 42.5 N.

FIGURE 2. Vibrating wire gauges under protective covers. Detail at one assembled location.

3.1. LONG-TERM MONITORING SYSTEM

A long-term monitoring system was designed and installed in one concrete pavement slab with dimensions of $3.5 \times 5.0 \times 0.29$ m. The system records temperature and strains at six measuring locations [25]. Each location contains three vibrating wire strain gauges located 50 mm from the surfaces and in the mid-height. All the gauges have integrated temperature sensors. In addition, one thermal gauge was placed 150 mm under the pavement in order to deliver the sub-base temperature. Ambient air temperature and solar radiation sensors were installed as well.

Two-lift concrete technology started with a bottom layer 240 mm thick with 370 kg/m^3 of the binder, following with the top layer 50 mm thick with 420 kg/m^3 of the binder. A two-step installation process was adopted, utilizing protective covers which hid the strain gauges before the casting, see Figure 2. After the first finisher had passed, the covers were removed, the gauges put in their positions and the empty space filled back with concrete using hand vibrators, see Figure 2. Finally, the top layer finalized the slab.

Almost $55\,000$ m^3 of concrete was placed in both layers, complying to required C30/37 strength class, see Figure 3.

Vibrating strain gauges measure relative head displacements, which can be decomposed to:

$$\varepsilon = \varepsilon_{ve} + \varepsilon_T + \varepsilon_{as} + \varepsilon_{ds} + \varepsilon_f + \ldots, \qquad (11)$$

where partial strains represent viscoelasticity, temperature effects, autogenous shrinkage, drying shrinkage, fracturing strain, etc.

Figure 4 shows partial strains on the mid-plane, zeroed at 2 hours after the end of setting for all gauges. Autogenous shrinkage plays a dominant role in the first week, reaching -70 µε in the transversal direction (W62). In the longitudinal direction, continuous casting led to prestressing, which adds additional strain. A small average drying shrinkage strain from -30 to -120 µε is apparent after 3 years of drying.

The measured strains allowed calculating the curvature of the slab, assuming a planar deformation of the cross-section. Figure 5 shows the total curvatures, capturing the temperature variations and demonstrating a slow positive drift due to top drying.
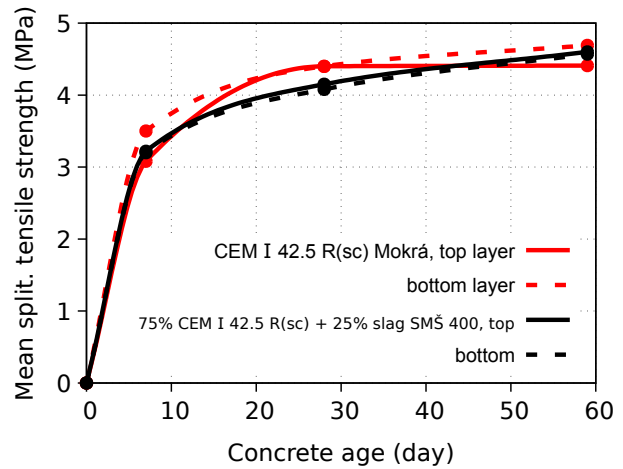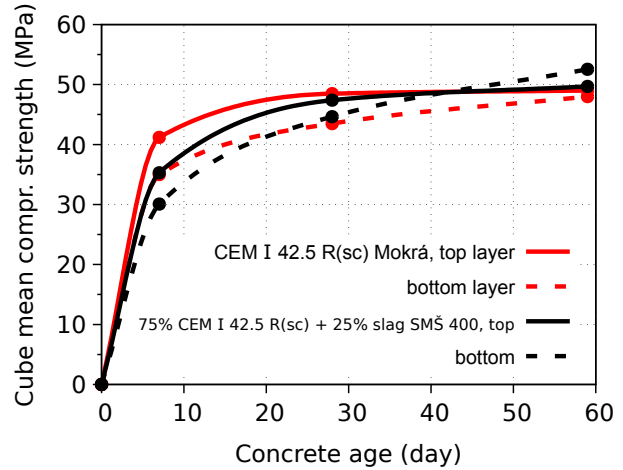

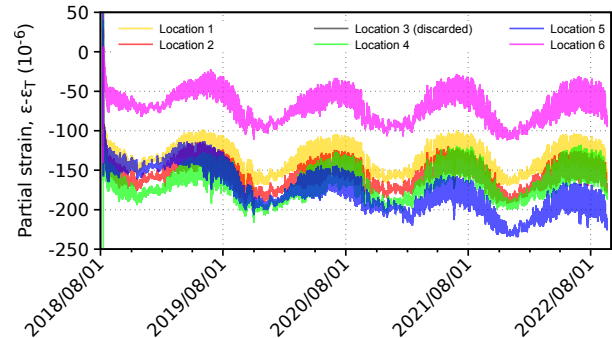FIGURE 3. Compressive and tensile strength evolution of top and bottom concretes.
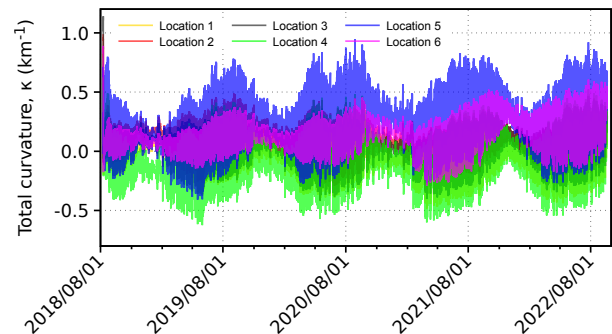

FIGURE 4. Partial strains on 6 locations.

FIGURE 5. Total curvatures at 6 locations.

	Parameter	Value	Unit	Parameter	Value	Unit
Mechanical model	$\overline{f}_c$	45.0	MPa	c_1	70.0	MNm^{-3}
	c_c cement content	370.0	$\mathrm{kg/m}^3$	c_2	60.0	MNm^{-1}
	w/c ratio	0.4	-	α	$10.0 \cdot 10^{-6}$	$°\mathrm{C}^{-1}$
	a/c ratio	4.91	-	k	200.0	MNm^{-1}
	t_0	7	days	k_3	35	-
	τ_1	$3 \cdot 10^{-5}$	days	τ_M	5000	days
	k_{sh}	$1.5 \cdot 10^{-3}$	-	E	35.0	GPa
	$\varepsilon^\infty_{sh,au}$	$-87.0 \cdot 10^{-6}$	-	ν	0.2	-
	τ_{au}	1.05	days	$R_{t,au}$	-4.5	-
	α_{au}	1.166	-			
Moisture transfer model	c_1	$6.0 \cdot 10^{-4}$	kg/m·s	α_0	1.0	-
	$k(h) = k_1$	160.0	$\mathrm{kg/m}^3$	β_{top}	0.05	$\mathrm{kg/m}^2 \cdot \mathrm{d}$
	β_{bottom}	0.01	$\mathrm{kg/m}^2 \cdot \mathrm{d}$			

TABLE 1. List of material input parameters.

3.2. SLAB GEOMETRY

The slab is meshed using 3D, quadratic, 20 node brick elements. Interaction between neighboring slabs is neglected. In moisture transfer simulation, the influence of air and soil is represented with Newton boundary conditions. The overview of used material parameters for concrete and subsoil is summarized in Table 1.

Parameters $\varepsilon^\infty_{sh,au,B4}$, τ_{au}, α_{au} and $R_{t,au}$ control the evolution of autogenous shrinkage. The basic creep in the MPS theory is influenced by the same four parameters q_1–q_4 as in the model B3, these are computed from $\overline{f}_c$, c_c, w/c and a/c. The units of solidifying Kelvin chain are defined with the lowest τ_1 and the highest retardation time τ_M. Time at the onset of drying is $t_0 = 7$ days (for lab experiment $t_0 = 0.1$ day), size effect for drying is neglected setting $p = \infty$.

3.3. HYGRO-MECHANICAL SIMULATION OF LONG-TERM SLAB DRYING

To simulate the long-term drying, the determination of material properties of concrete and relevant boundary conditions are necessary. Material properties used in this paper are derived from drying shrinkage lab experiments. The kinetics of slab drying can be estimated from small lab samples 60×100 mm exposed to 50 % RH from the largest side. Permeability (and hygric exchange coefficient) was calibrated from moisture transport model.

Boundary conditions are derived from a 40 year old concrete slab, which was removed during the demolition of D1 highway. The thickness of the old slab is only 240 mm compared to 290 mm used in current simulation. The moisture profile (see Figure 6) and the fully saturated state were determined. We assume that the drying process is stabilized after 40 years, which identified ambient relative humidity as 65 % at the top and 80 % at the bottom.

Moisture transfer coefficients ($\beta_{\mathrm{top}} > \beta_{\mathrm{bottom}}$) are set in such a way that the top drying becomes dominant. The linear moisture profile from Figure 6 also implies that the permeability needs to stay constant, otherwise non-linear profile is obtained. The explanation for this phenomenon is likely a sorption isotherm and full resaturation with rain water. It was showed on prisms, that rewetting is orders of magnitude faster process than drying, thus occasional rain will lead to linear moisture profile [26]. This leads to setting $\alpha_0 = 1$ and $c(h) = c_1$ according to Equation (2).

Figure 7 shows shrinkage validation of numerical model both for lab experiment and for concrete pavement (strain gauge W52).

The strain from gauge W52 was shifted by 40 με to eliminate longitudinal prestressing. The predictions show that the slab will be drying for approximately 30 years. It should be mentioned that other gauges show smaller mid-plane shrinkage values, attributed likely to other partial strains and restraints.

The initial drying takes place predominantly in top and bottom 100 mm of the slab, see Figure 6. This leads to stress induction in these areas and subsequent redistribution in time. The early age stress field (first 2 years) shows tensile stress in the top part of the slab (around 3.3 MPa after 60 days and 2.2 MPa after 1 year, see Figure 6). This will likely cause cracking in the slab when combined with temperature and traffic load. Concrete slab should be able to cope with the resulting fracture process zone since the slab is continuously supported and controlled by displacement to a large extent. Similar stresses were found on the analysis of restrained slab with thermo-hygro-mechanical model; exposing 150 mm thick slab to 60 % RH led to tensile stresses up to 3 MPa after 100 days [27].
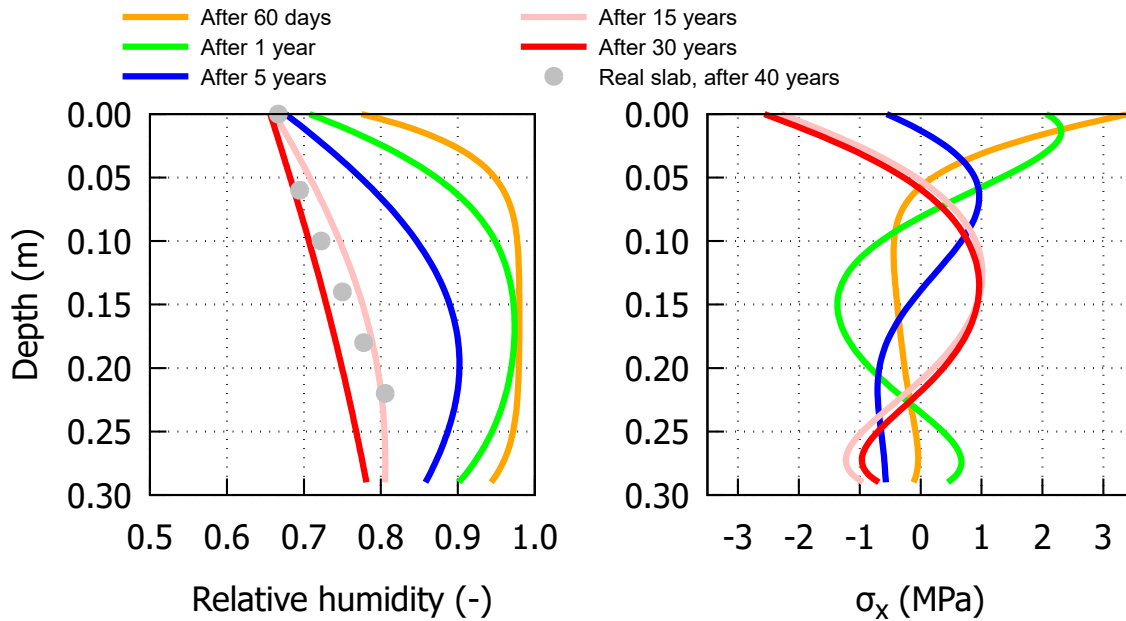
Figure 6. Comparison of relative humidity profile (left) from FE simulation with real slab data after 40 years and σ_x (right) induced by long term drying.
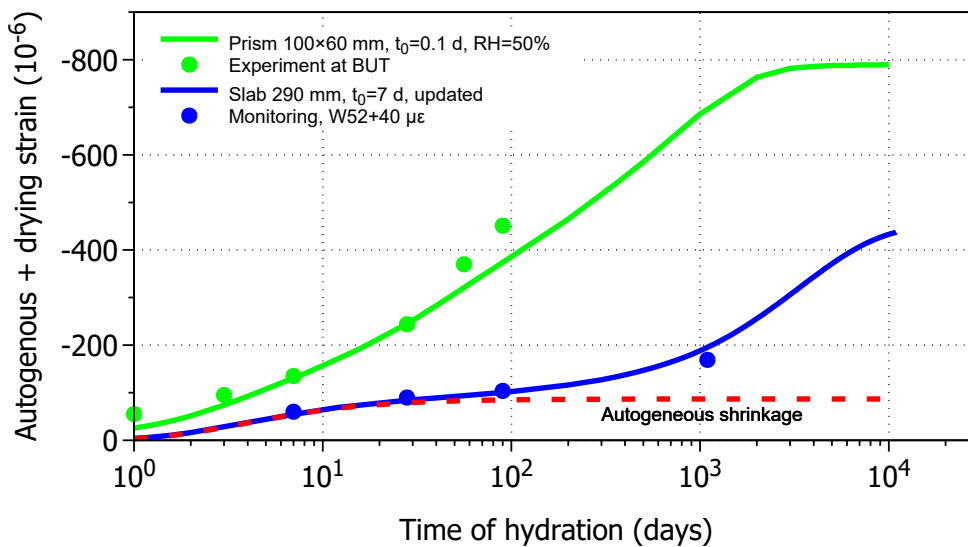

Figure 7. Shrinkage validation of concrete slab with monitoring.

After 2 years, the compression occurs within the top layer and the tensile stress occurs in the middle of the slab. The tensile stress reaches values up to 1.0 MPa, these are values lower than tensile strength of the concrete. The compression of the top layer of concrete is likely to help close the cracks developed in the earlier phase.

The deformed shape induced by long-term drying is known as warping. The simulation predicts that the corners will raise up up to 1.7 mm when subjected to drying and self-weight (see Figure 8).

4. Conclusions

This paper describes behavior of road concrete slab when subjected to the long-term drying. Individual material models were calibrated based on lab and field

experimental data, the main source being a long-term monitoring system on D1 highway. Shrinkage was validated both for lab experiment and for the concrete pavement with moisture transport model. Boundary conditions were calibrated from moisture profile of 40 year old pavement. Drying induces high tensile stress on top surface, reaching 3.3 MPa after 60 days and 2.2 MPa after 1 year of drying. As the drying front advances, the stress profile changes and the surface becomes slightly compressed. Slab warping is predicted as 1.7 mm corner uplift at the maximum.
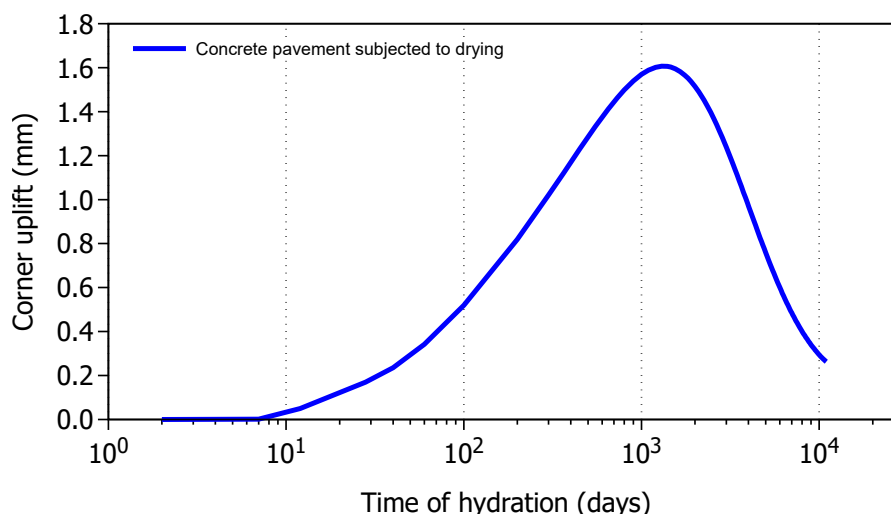
FIGURE 8. Warping induced by long-term drying of concrete.

REFERENCES

[1] M. G. Lay. *Handbook of road technology.* CRC Press, 2009.

[2] T. Gasch, R. Malm, A. Ansell. A coupled hygro-thermo-mechanical model for concrete subjected to variable environmental conditions. *International Journal of Solids and Structures* **91**:143–156, 2016. https://doi.org/10.1016/j.ijsolstr.2016.03.004

[3] V. Sadeghi, S. Hesami. Investigation of load transfer efficiency in jointed plain concrete pavements (JPCP) using FEM. *International Journal of Pavement Research and Technology* **11**(3):245–252, 2018. https://doi.org/10.1016/j.ijprt.2017.10.001

[4] Y. Dere, A. Asgari, E. D. Sotelino, G. C. Archer. Failure prediction of skewed jointed plain concrete pavements using 3D FE analysis. *Engineering Failure Analysis* **13**(6):898–913, 2006. https://doi.org/10.1016/j.engfailanal.2005.07.001

[5] P. Mackiewicz. Thermal stress analysis of jointed plane in concrete pavements. *Applied Thermal Engineering* **73**(1):1169–1176, 2014. https://doi.org/10.1016/j.applthermaleng.2014.09.006

[6] L. Bronuela, H. "David" Lee, S. Ryu, Y. Ho Cho. Cantilever and pull-out tests and corresponding FEM models of various dowel bars in airport concrete pavement. *Construction and Building Materials* **83**:181–188, 2015. https://doi.org/10.1016/j.conbuildmat.2015.02.066

[7] K. Singh, G. Ghosh. Stress behavior of concrete pavement. *Materials Today: Proceedings* **55**:246–249, 2022. https://doi.org/10.1016/j.matpr.2021.06.424

[8] Z. Lyu, Y. Guo, Z. Chen, et al. Research on shrinkage development and fracture properties of internal curing pavement concrete based on humidity compensation. *Construction and Building Materials* **203**:417–431, 2019. https://doi.org/10.1016/j.conbuildmat.2019.01.115

[9] X. Zhang, H. Zhao. Characterization of moisture diffusion in cured concrete slabs at early ages. *Advances in Materials Science and Engineering* **2015**:154394, 2015. https://doi.org/10.1155/2015/154394

[10] J.-H. Jeong, D. G. Zollinger. Environmental effects on the behavior of jointed plain concrete pavements. *Journal of Transportation Engineering* **131**(2):140–148, 2005. https://doi.org/10.1061/(ASCE)0733-947X(2005)131:2(140)

[11] S. Liang, Y. Wei, Z. Wu, W. Hansen. Performance evaluation of concrete pavement slab considering creep effect by finite element analysis. *Transportation Research Record* **2672**(27):65–77, 2018. https://doi.org/10.1177/0361198118772951

[12] V. Malárics, H. S. Müller. Numerical investigations on the deformation behavior of concrete pavements. In *7th RILEM International Conference on Cracking in Pavements*, pp. 507–516. Springer, 2012. https://doi.org/10.1007/978-94-007-4566-7_49

[13] L. Jendele, V. Šmilauer, J. Červenka. Multiscale Hydro-thermo-mechanical Model for Early-Age and Mature Concrete Structures. *Advances in Engineering Software* **72**:134–146, 2014. https://doi.org/10.1016/j.advengsoft.2013.05.002

[14] D. Gawin, F. Pesavento, B. A. Schrefler. Hygro-thermo-chemo-mechanical modelling of concrete at early ages and beyond. Part I: Hydration and hygro-thermal phenomena. *International Journal for Numerical Methods in Engineering* **67**(3):299–331, 2006. https://doi.org/10.1002/nme.1615

[15] D. Gawin, F. Pesavento, B. A. Schrefler. Hygro-thermo-chemo-mechanical modelling of concrete at early ages and beyond. Part II: shrinkage and creep of concrete. *International Journal for Numerical Methods in Engineering* **67**(3):332–363, 2006. https://doi.org/10.1002/nme.1636

[16] F. Kanavaris, C. Ferreira, C. Sousa, M. Azenha. Thermo-chemo-hygro-mechanical simulation of the restrained shrinkage ring test for cement-based materials under distinct drying conditions. *Construction and Building Materials* **294**:123600, 2021. https://doi.org/10.1016/j.conbuildmat.2021.123600

[17] B. Patzák. OOFEM project home page, since 2000.
CTU in Prague, Faculty of Civil Engineering.
[2022-10-13]. http://www.oofem.org

[18] W. Dong, C. Liu, X. Bao, et al. Advances in the
deformation and failure of concrete pavement under
coupling action of moisture, temperature, and wheel
load. *Materials* **13**(23):5530, 2020.
https://doi.org/10.3390/ma13235530

[19] M. Jirásek, P. Havlásek. Microprestress-solidification
theory of concrete creep: Reformulation and
improvement. *Cement and Concrete Research* **60**:51–62,
2014.
https://doi.org/10.1016/j.cemconres.2014.03.008

[20] Z. Bažant, S. Baweja. Short form of creep and
shrinkage prediction model B3 for structures of medium
sensitivity. *Materials and Structures* **29**:587–593, 1996.
https://doi.org/10.1007/BF02485965

[21] P. Havlásek, M. Jirásek. Multiscale modeling of
drying shrinkage and creep of concrete. *Cement and
Concrete Research* **85**:55–74, 2016.
https://doi.org/10.1016/j.cemconres.2016.04.001

[22] A. C. Lamprea-Pineda, D. P. Connolly, M. F. M.
Hussein. Beams on elastic foundations – A review of
railway applications and solutions. *Transportation
Geotechnics* **33**:100696, 2022.
https://doi.org/10.1016/j.trgeo.2021.100696

[23] B. J. S. Breeveld. *Modelling the Interaction between
Structure and Soil for Shallow Foundations –
A Computational Modelling Approach.* Ph.D. thesis,
Delft University of Technology, 2013.

[24] D. Younesian, A. Hosseinkhani, H. Askari,
E. Esmailzadeh. Elastic and viscoelastic foundations:
a review on linear and nonlinear vibration modeling and
applications. *Nonlinear Dynamics* **97**(1):853–895, 2019.
https://doi.org/10.1007/s11071-019-04977-9

[25] B. Slánský, V. Šmilauer, J. Hlavatý, R. Dvořák. New
Long-Life Concrete Pavements in the Czech Republic.
In *12th International Conference on Concrete
Pavements*, pp. 228–239. 2021.

[26] L. Dohnalová, P. Havlásek, V. Šmilauer. Behavior of
predried mature concrete beams subject to partial
wetting and drying cycles. *Acta Polytechnica CTU
Proceedings* **34**:1–5, 2022.
https://doi.org/10.14311/APP.2022.34.0001

[27] J. Gomes, R. Carvalho, C. Sousa, et al. 3D numerical
simulation of the cracking behaviour of a RC one-way
slab under the combined effect of thermal, shrinkage and
external loads. *Engineering Structures* **212**:110493, 2020.
https://doi.org/10.1016/j.engstruct.2020.110493